S. Oktay

Multi-fluid Subdued Boiling; Theoretical Analysis of Multi-fluid Interface Bubbles

Abstract: The recently discovered boiling phenomenon called "multi-fluid subdued boiling" is discussed. It has been observed that when a beaker containing two immiscible liquids of dissimilar densities is heated at the bottom, the vapor bubbles rise in the lower liquid until they reach the liquid-liquid interface. There the bubbles are trapped, and after a short period of time they collapse. As the heat transfer is increased, however, the bubbles begin to coalesce to form a new set of "interface bubbles," and the latter eventually become large enough to break away from the interface and rise into the upper liquid layer. Upon reaching the liquid-air interface most of the bubbles do not escape into the ambient but suddenly condense, contract and drop back toward the lower liquid level. "Boiling off," or net vapor generation, is subdued.

The prediction of the interface bubble sizes is also discussed. Analysis shows that the properties of the fluids used can be included mathematically in nondimensional parainetric forms, by means of which the shapes and sizes of the interface bubbles can be found.

Nomenclature

A	an undetermined coefficient of the "exterior" solution
C_p	specific heat
F	a dimensionless coordinate
f	axi-symmetric surface function
h	heat transfer coefficient
H	latent heat
G	gravitational constant
Ja	Jakob number ($\rho C_p \Delta T/\rho_v H$)
k	thermal conductivity
K_0	Bessel function of order zero
K_1	Bessel function of order one
Nu	Nusselt number ($h2r_0/k$)
$\mathbf{n}$	unit normal to surface
$n_{1,2,3}$	components of unit normal
Pe	Péclét number ($v2r_0/\alpha$)
p	pressure
p_{ext}	external liquid pressure
$p_{o,c}$	pressure at the origin of the "cup"
$p_{o,d}$	pressure at the origin of the "dome"
p_v	vapor pressure within a bubble
R	dimensionless radius
R_c	radius of curvature at the origin of the "cup"
R_d	radius of curvature at the origin of the "dome"
r	radius
r_m	match point radius
r_0	maximum bubble radius
T	temperature
v	bubble velocity
$x_{1,2,3}$	cartesian coordinates
ΔZ	relative elevation (Fig. 17)
α	thermal diffusivity
β_c	a non-dimensional parameter for the "cup" solution
β_d	a non-dimensional parameter for the "dome" solution
ζ	dimensionless radial coordinate for the "exterior" region
θ	angle
ρ	mass density
σ	surface tension
σ_l	surface tension of lower (primary) liquid
σ_u	surface tension of upper (secondary) liquid
σ_{lu}	interfacial surface tension between upper and lower liquids
Φ	dimensionless elevation coordinate for the "exterior" region
Φ_e	a non-dimensional parameter for the "exterior" solution
$(')$	notation for differentiation

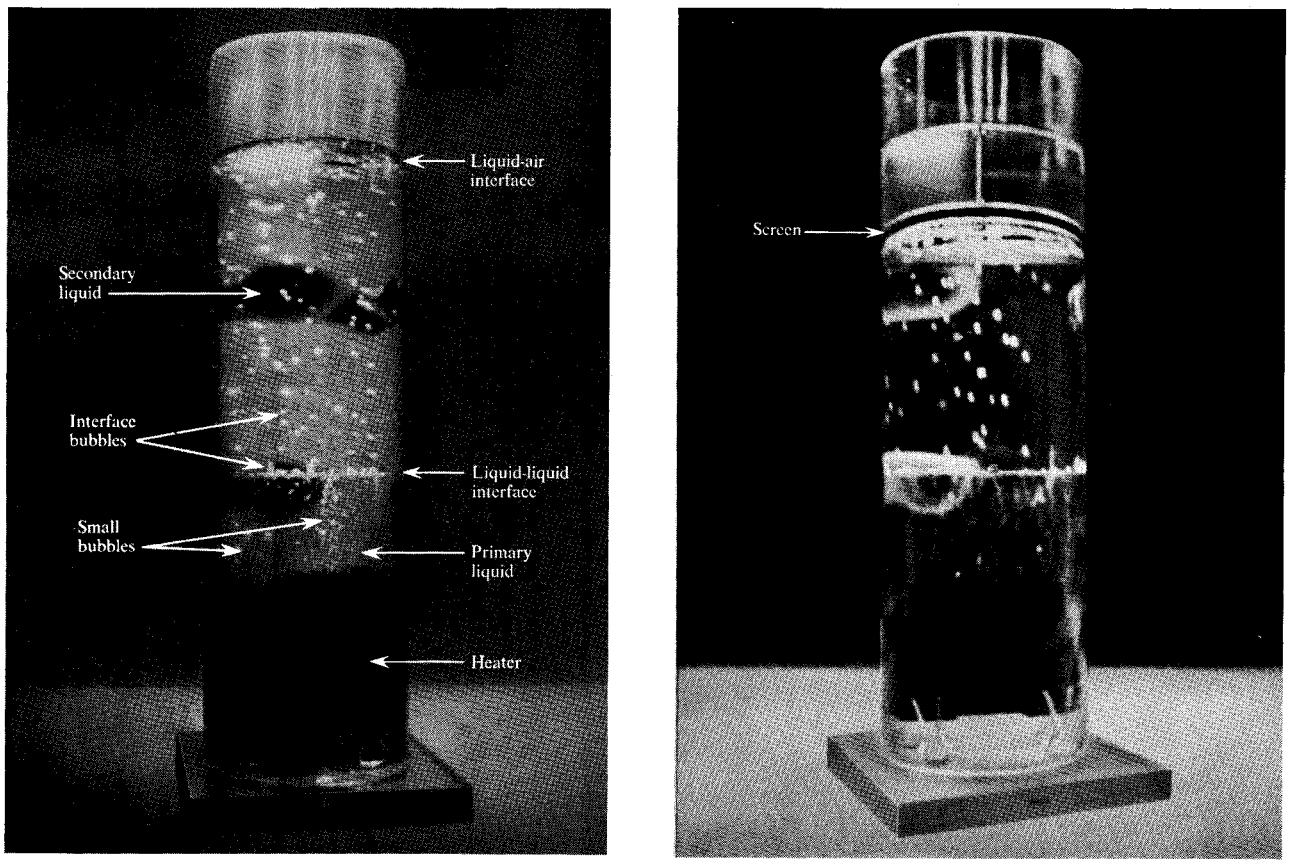

(a) (b)

Figure 1 Multi-fluid boiling experiment: (a) Bubbles reach liquid-air interface and condense; (b) bubbles condense at screen.

Introduction

In some electronic components in high speed computers it is possible to encounter power densities in excess of 15 watts-cm^{-2}. At such high densities it may be necessary to use a vaporization mode of heat transfer in which a properly selected material changes phase. For example, with subcooled local boiling, high rates of heat transfer are possible. Even higher rates of heat transfer can be obtained with a nucleate boiling mode[1]. However, usually any single-fluid boiling results in vapor bubbles and net vapor generation which render it undesirable in some applications.

The following is a description of a novel method of cooling called multi-fluid subdued boiling* which yields high heat transfer rates but with negligible, if any, net vapor generation. This is accomplished by superimposing immiscible liquids in such a way that the heat generating components are completely submerged in the bottom-layer liquid (see Fig. 1). Then the vapor bubbles emanating from the heated surfaces rise to the liquid-liquid interface and, under certain conditions, may condense there. They will also condense in the upper-layer liquid, but only after a new set of bubbles, called interface bubbles, is formed from them as they traverse the boundary between the two different media. That mechanism is more fully described later in this paper.

Although heat, mass and momentum transfer across surfaces of separation between immiscible liquids have been of interest to researchers and a great deal of work has been done in this area, no information has been reported in the literature pertaining to the mechanisms governing the behavior of multi-fluid subdued boiling phenomena. However, some related work that may be relevant to multi-fluid boiling will be mentioned briefly in the next section.

The mechanisms are not well understood. To assist in the understanding, a method of predicting the size of the interface bubbles formed at the surface of separation between two immiscible liquids is also presented. The analysis shows that the size as well as the shape of the interface bubbles can be predicted as functions of cer-

*S. Oktay, U.S. Patent No. 3,406,244; October 15, 1968.

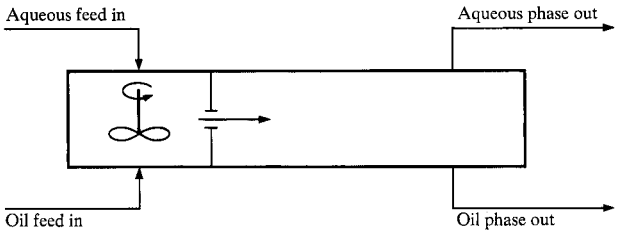

Figure 2 Direct-contact heat exchanger for immiscible liquids using mixer-settler contactor. (After Ref. 9.)

tain non-dimensional parameters containing the properties of the fluids used.

The multi-liquid systems that are reported here are Water/FC-78* and Coolanol 45†/FC-78. It should be pointed out that in immersion cooling, the liquids must be compatible with the packaging materials, which may be different for different applications. The liquids as well as the cooling systems that are discussed here are included for illustrative purposes.

Heat exchange between immiscible liquids

Recently, there has been some work devoted to developing heat exchangers in which heat is transferred by direct contact between immiscible liquids. This involves the deliberate mixing and, after heat exchange takes place between the dispersed liquids, separation of the liquid phases to repeat the process (Fig. 2). Such a system offers the advantage that, in the absence of a separating wall between the two liquid phases, the thermal resistance associated with the walls of a conventional heat exchanger is eliminated. This approach seems to be especially attractive where corrosive or fouling liquids are processed, since the interfacial heat exchange surface is continuously renewed and scaling problems do not arise. It is also expected that due to the intimate dispersion of the liquid droplets, high rates of heat transfer should be attainable. For example, Sideman and Taital have reported overall heat transfer coefficients of the order of 0.5 cal-sec^{-1}-cm^{-2}-°C^{-1} for evaporating single droplets of butane and pentane is distilled water[2]. For three immiscible liquid mixtures on a horizontal heated plate where the lower liquid exhibts film boiling, Bragg and Westwater[3] have found greater heat transfer rates than for the lower liquid alone, due to the presence of the cooler upper liquid.

Experimental and theoretical investigations of boiling from liquid surfaces have also been reported. In this arrangement, the lighter volatile liquid on top is heated by the lower immiscible liquid with boiling of the top liquid occurring at the plane of contact. Viskanta and Lottes[4] have demonstrated that in boiling from a liquid surface the chemical nature of the liquid-liquid interface changes the degree of liquid superheating that can be attained at the surface. Fortuna and Sideman[5] have also studied the problem of heat transfer at the liquid-liquid interface. Taking it one step further, they stirred the liquids in order to study the effects of forced convection mechanisms on the heat transfer between two liquid layers.

In still another paper Isenberg and Sideman[6] have investigated direct contact three-phase heat exchangers, in which one liquid undergoes phase change while dispersed in another immiscible liquid. Their study showed that heat transfer with change of phase provides the advantage of smaller flow rates in the transfer fluid, convenient separation of the fluids, and very high heat-transfer coefficients. They have also shown that for a given initial bubble size the rate of collapse of bubbles is faster in a two-component (multi-fluid) system than that obtained in the corresponding single component system. Similar findings in multi-fluid boiling have been reported by the author[7].

Experimental observations of bubble dynamics and heat transfer in multi-fluid subdued boiling

In multi-fluid subdued boiling the liquids are not dispersed. As shown in Fig. 1, immiscible liquids of dissimilar densities are placed in a container. The liquid on top, which we shall call the secondary liquid, has a boiling point and specific heat higher than that of the primary liquid, which is at the bottom. Typical properties of some of the liquids are shown in Table 1.

When a component such as a resistor heater is immersed in the primary liquid and powered, vapor bubbles form on the heated surface. Then the bubbles rise in the primary liquid until they reach the liquid-liquid interface. There the bubbles no longer continue their ascent into the upper-layer secondary liquid, but instead begin to move horizontally in the plane of the interface. In effect, the bubbles become trapped at the interface, and after a short period of time they collapse.

As the heat is increased, however, the bubbles at the interface begin to coalesce (see Fig. 3), forming what we have called interface bubbles. The bubbles so formed eventually become large enough to break away from the interface (see Fig. 4, taken from a high speed motion picture) and rise into the upper liquid. Upon reaching the free liquid-air interface, however, most of the bubbles do not escape into the ambient. On the contrary, they suddenly condense, contract and drop back toward the lower primary liquid. In other words, "boiling off" (or net vapor generation) is subdued.

*FC-78 is a fluorocabon liquid made by 3M Company.
†Coolanol 45 is a silicate ester made by Monsanto Company.

Furthermore, the dropping bubbles either collapse completely within the bulk of the upper liquid, or continue contracting in abrupt stages until they become very small. Still others, as they drop back down through the secondary liquid, form crescent-shaped "doublets" [Fig. 5(a)] which seem to contain both the liquid and the gas phase of the primary liquid, thereby suggesting condensation in the secondary liquid. If more than two layers of fluid are used, the bubbles undergo more intricate nucleation, one example of which is shown in Fig. 5(b).

The nature of bubble growth and bubble dynamics at the liquid-liquid interface becomes important both from the point of view of heat transfer across the interface and from that of heat transfer from the interface bubbles to their liquid environment. As mentioned earlier, with direct liquid to liquid contact the thermal resistance commonly encountered between the wall of a heat exchanger and the liquids that it separates is removed. Heat transfer across the liquid-liquid interface is further enhanced by the dynamics of the replenishment of liquid in the region occupied by an interface bubble prior to disengagement from the interface. If, in addition, forced convection of the secondary liquid is superimposed at the interface, high heat transfer rates can be obtained. As an example, the forced convection approach can be arranged as shown in Fig. 6.

The figure depicts a box containing an electronic component, say a memory unit. The component is completely submerged in a dielectric coolant. The secondary liquid on top is circulated through a remote heat exchanger. The liquid returning from the heat exchanger is reintroduced into the box via a manifold containing several holes. The opening at the outlet would normally have a screen (not shown in Fig. 6) to prevent bubbles from entering the heat exchanger. Also, the outlet is preferably located below the free surface, where most of the bubbles congregate before they condense and fall back down.

In effect, the secondary liquid in Fig. 6 replaces a cold plate which would normally be required to condense bubbles in a conventional sealed unit. As expected, the motion of the bubbles in the secondary liquid effects the condensation of the interface bubbles. It is found that the condensation occurs at low driving forces. In other words, the temperature of the secondary liquid may be very close to that of the vapor inside the bubble (the saturation temperature of the primary liquid), and yet the interface bubbles continue collapsing within the bulk of the secondary liquid. This may be explained by the effect of motion on heat transfer. Isenberg et al[6] show this coupling effect via the interrelationship between Péclét (*Pe*) and Jakob (*Ja*) numbers. At higher *Pe* numbers, corresponding to large bubbles with high velocities such as the typical interface bubble, the bubble collapse

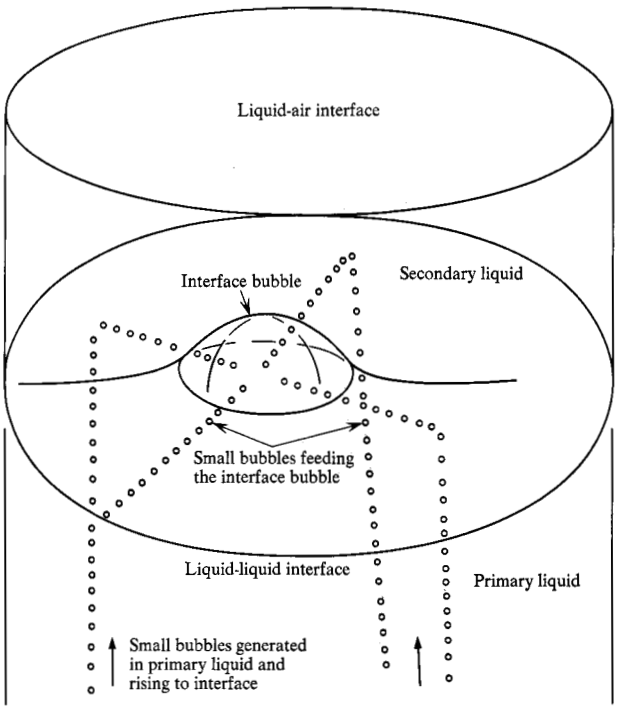

Figure 3 Interface bubble formation.

Table 1 Properties of typical liquids used in multi-fluid boiling.

	Primary liquids		*Secondary liquids*	
	*FC-78**	*FC-88**	*Coolanol 45†*	*Water*
Nominal boiling point (°C)	51	32	–	100
Vapor pressure at 25°C (mm Hg)	260	570	0.01	0.26
Density at 25°C ($g\text{-}cm^{-3}$)	1.7	1.6	0.89	1
Heat of vaporization at the boiling point ($cal\text{-}gm^{-1}$)	41	20.4	–	540
Thermal conductivity at 25°C ($cal\text{-}sec^{-1}\text{-}cm^{-1}\text{-}°C^{-1}$)	0.00014	0.00014	0.00035	0.001
Specific heat at 25°C ($cal\text{-}g^{-1}\text{-}°C^{-1}$)	0.24	0.24	0.46	1
Surface tension at 25°C ($dynes\text{-}cm^{-1}$)	13	13	26	72
Dielectric constant at 25°C, 1kHz	–	1.81	2.60	80

*Made by 3M Co.
†Made by Monsanto Co.
Note: Any one of the primary liquids is immiscible with any one secondary liquid. Recent work indicates that secondary liquids are soluble in primary liquids to some extent.

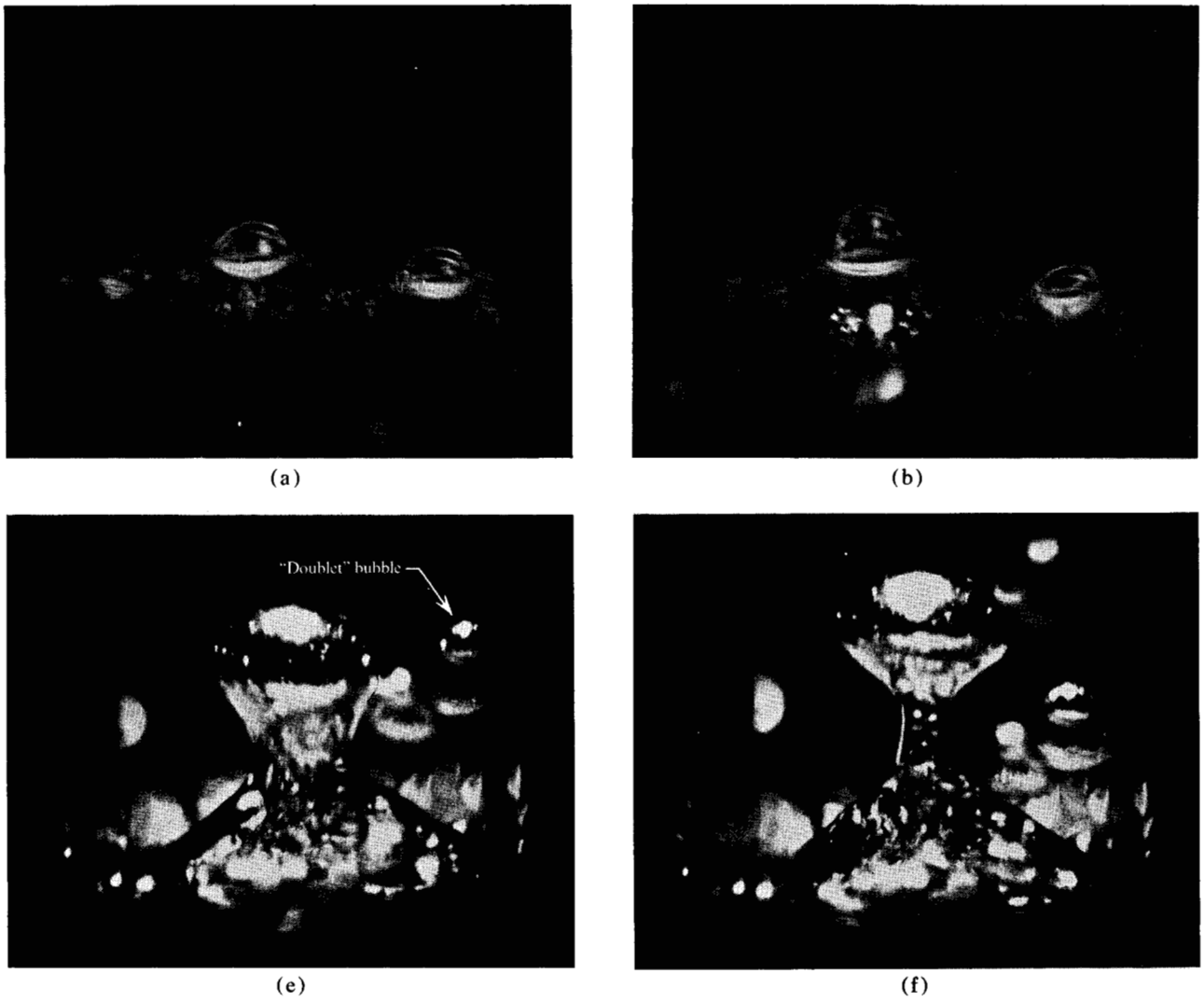

Figure 4 (Above and opposite) High-speed motion picture frames showing the formation of an interface bubble.

Figure 5 Bubble formations: (a) "Doublet" formed in two-layer liquid boiling; (b) "paired-doublet" formed in three-layer liquid boiling.

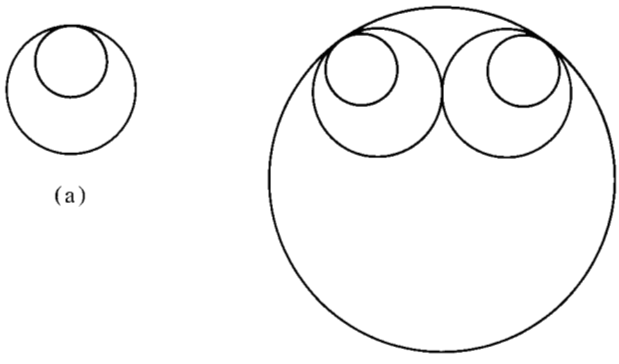

is faster because the convection rates are higher. Consequently, with high Pe it is possible to have bubble collapse even with low Ja numbers, i. e., with a small driving force ΔT between the bubble and its liquid environment.*

In addition, it should also be noted that the heat transfer rate from a bubble is controlled by the liquid surrounding the condensing bubble. Since the thermal properties of the secondary liquid are more favorable than that of the primary liquid (compare the thermal conductivities in Table 1), it is expected that the condensation in the secondary liquid will be faster than in the primary liquid. Thus for FC-78 bubbles in water, the experimental bubble heat transfer coefficient is $\approx$ 0.1 cal-sec^{-1}-cm^{-2}-°C^{-1}, and is to be compared with a value of 0.16 cal-sec-cm^{-2}-°C^{-1} as obtained from the relationship

*Typically $Pe = 5000$, $Ja = 45$ for water/FC-78 system.

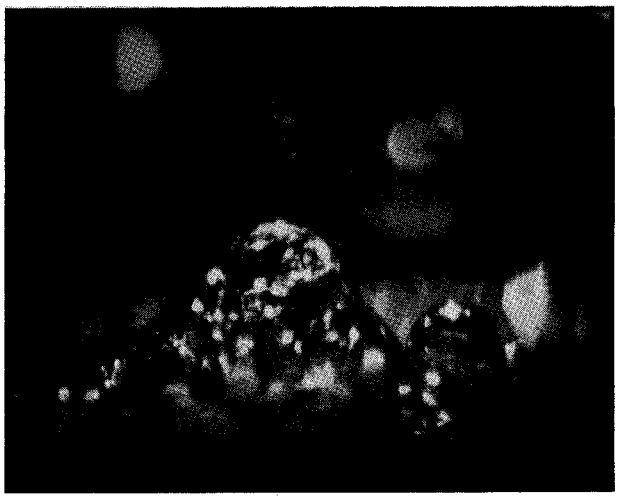

(c)

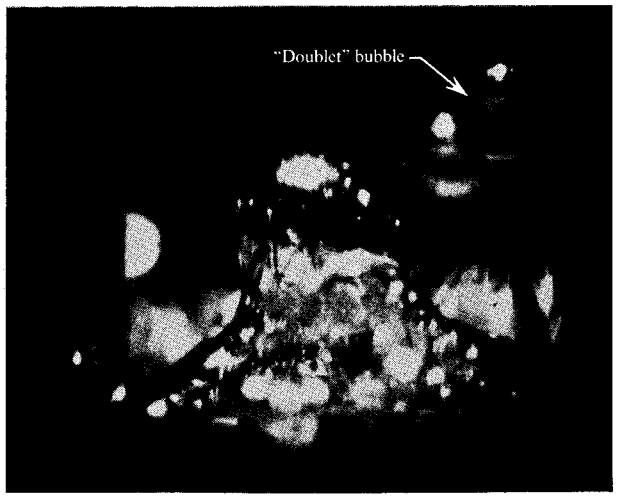

(d)

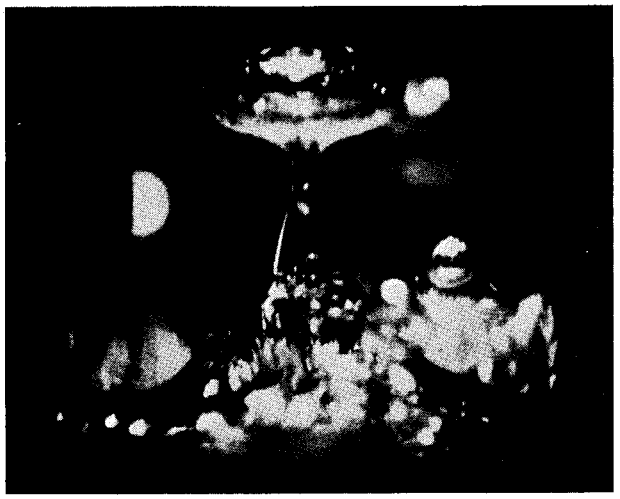

(g)

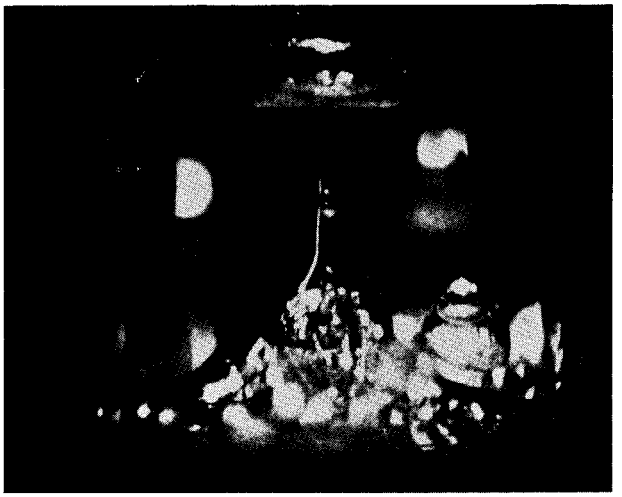

(h)

$Nu/Pe^{1/2} = 0.5$[5]. This is approximately an order of magnitude higher than that found for FC-78 bubbles in FC-78 liquid.

The bubble diameter ($\approx$ 5 mm) and the bubble velocity ($\approx$ 40 mm-sec^{-1}) that enter into the calculations were measured from a high speed motion picture taken by a Fairchild camera, Model No. HS401. The ΔT ($\approx$ 3°C) was obtained by assuming the bubble vapor temperature to be the same as the saturation temperature of the primary liquid and subtracting the measured secondary liquid temperature from it. The effect of the presence of noncondensables, such as air, on the bubble temperature is neglected.

The mechanism of heat transfer between the interface bubbles and the secondary liquid is complicated by the fact that both mass and heat transfer are taking place simultaneously, both inside and outside the bubble as in

Figure 6 Direct-flow system.

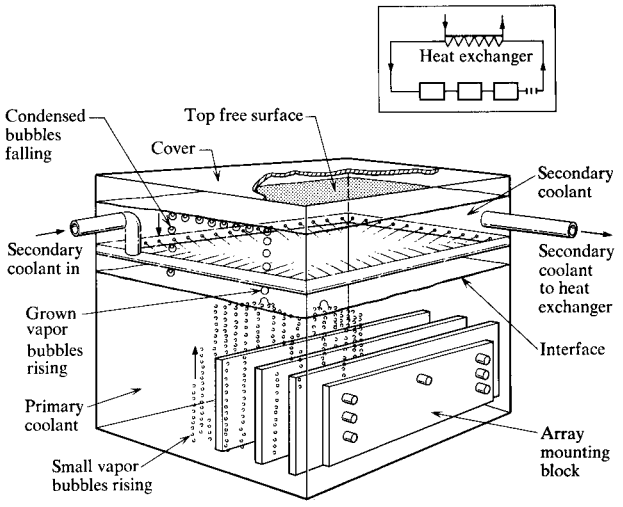

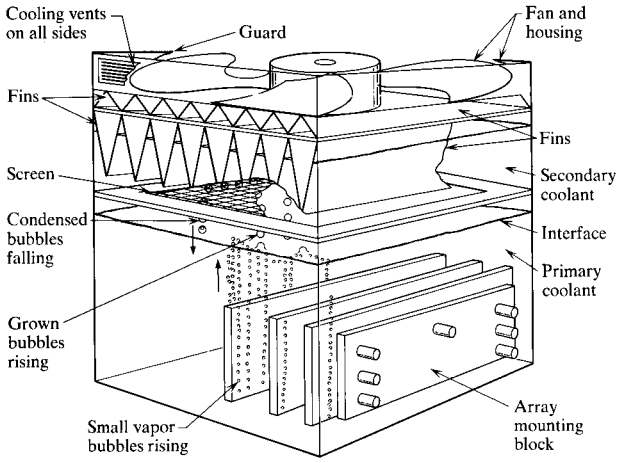

Figure 7 No-flow system.

Figure 8 Modular multi-fluid air cooling system.

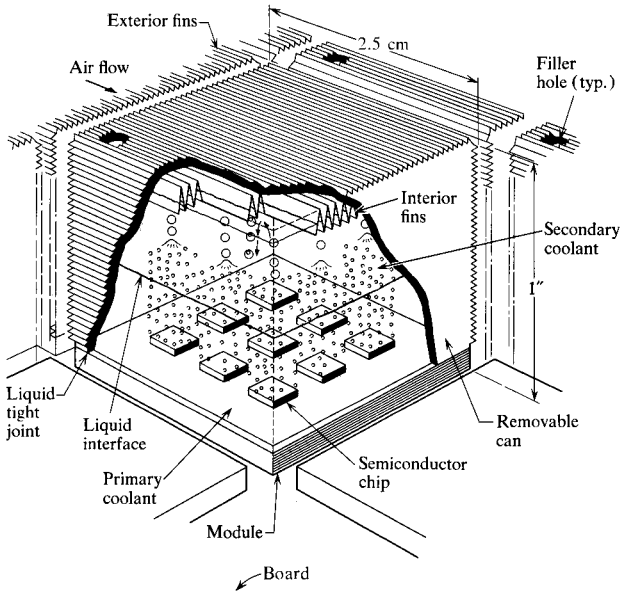

the case of the "doublet" mentioned previously. However, it can be said that the interface bubble condensation is similar to that of "dropwise condensation." This is because, as the interface bubbles move through the secondary liquid, they remain distinct; when they condense, the condensation occurs in the form of partial droplets. Thus the condensing vapor, which is already in the form of bubbles, cannot coalesce to form a film condensate within the condenser liquid, namely the secondary liquid. In comparison, on a conventional metal condenser surface "film condensation" can occur and, as is known, the heat transfer coefficients are approximately an order of magnitude less than those obtained with "dropwise condensation".

Due to the high heat transfer coefficients at the vapor-liquid interface, vapor bubble condensation can be achieved with small temperature differences between the vapor inside the bubble and the surrounding secondary liquid. Thus, the interface bubbles can condense in a secondary liquid environment of wide temperature range provided that the surrounding temperature does not exceed the saturation temperature of the vapor inside the bubble. Hence, from a systems application viewpoint, several boxes can be tied together serially without effecting the condensation of the bubbles from one box to another, although the temperature of the secondary liquid may vary considerably from the first box to the last one (see inset in Fig. 6). On the other hand, in single-liquid boiling, where cold plates may be used in each box for condensing the bubbles, not as many of the same boxes may be cooled serially because of the much smaller allowable temperature rise in the coolant in each cold plate.

At certain power levels, the interface bubbles condense or collapse within the secondary liquid before they reach the free liquid-air interface. At relatively low power levels on the other hand, the interface bubbles invariably reach the top liquid surface before condensing. The mechanism of bubble collapse at the free surface is not well understood.

In the case for which a liquid-sold interface is substituted for a liquid-air interface (as with the interior fins in Fig. 7) it is found that heat transfer from the bubble to the solid surface is aided by the heat-conductive liquid surrounding the bubble. The bubbles may also be prevented from contacting the solid surface. In Fig. 7 this is done by placing a screen in the secondary liquid below the tips of the fins. Note that the cover of the box in Fig. 7 has fins on both sides of it. Interior fins dip into the secondary liquid so that heat is conducted away from the interior of the box to the top of the box. The heat is force-convected by means of a fan fitted to the top of the box. The advantage of this scheme over the one shown in Fig. 6 is that the box can be air cooled; furthermore each box can be serviced independently of others.

A possible use of multi-fluid subdued boiling in electronic module cooling[8] is depicted in Fig. 8. Here again the liquid-air surface is replaced by a liquid-solid interface. The modular box itself is air-cooled whereas the electronic devices in it are liquid cooled. In this illustration the box is approximately a 2.5 cm cube, and it contains nine semiconductor chips. Assuming that each chip has an effective area of 0.25 cm × 0.25 cm and that each chip dissipates 3 watts, we can determine chip power density to be 48 watts-cm^{-2}, a value that requires vaporization cooling. On the other hand, the total module power dissipation is 27 watts. With the cubical finned metal can shown in Fig. 8, the power density at

the module level can be reduced to less than 0.5 watts-cm^{-2}. Then the module can be air-cooled without excessive temperature rise between the ambient air and the can. With an FC-78/Coolanol 45 system, the required air temperature is approximately 30°C. This is based on an experimental condensation coefficient of 0.03 cal-sec^{-1}-cm^{-2}-°C^{-1} for FC-78 vapor bubbles in Coolanol 45.

As pointed out earlier, the size of the interface bubbles influences the heat transfer rates and their formation uniquely characterizes the multi-fluid subdued boiling phenomenon. It is of interest, therefore, to be able to predict the size and shapes of the interface bubbles. The analysis that follows immediately below shows that the size and shape of the interface bubbles can be predicted as funtions of certain non-dimensional parameters containing the properties of the fluids used. Laplace's equation has been solved on an IBM 7090 computer for axi-symmetric surfaces of separation formed at the interface of the two fluids. The resulting families of integral curves are matched subject to bubble compatibility conditions at the liquid-liquid interface. Finally, the largest bubble size that can be supported at a given liquid-liquid interface has been determined by an iterative procedure. The calculated results are in good agreement with measured bubble sizes in water and FC-78 fluorochemical liquid as determined from an experimental multi-fluid subdued boiling system.

Analysis of multi-fluid interface bubbles

Consider an interface bubble just prior to disengagment (see Fig. 4) from the liquid-liquid interface. In Fig. 9, the bubble is divided into several sections where the arc element ABC forms the upper portion of the bubble, or the "dome." The lower portion of the bubble is formed by the arc CDA, or the "cup." The lower fluid L rises above interface and surrounds the bubble until it becomes only a thin layer at A and C. The outer boundaries of fluid L near the bubble are determined by the "exterior" curves AX and CX, which asymptotically extend into the liquid-liquid interface. Note that as the bubble grows, points A and e and points C and f move toward each other, eventually coalescing at bubble disengagement.

It is clear that the vapor inside the interface bubble is that of fluid L, since the bubbles that "feed" the interface bubble originate from a heated object in fluid L. Assuming that the bubble is axi-symmetric and that the dynamics of fluid motion in the region between the "exterior" curves and the "dome" are negligible, we can find the shape and size of bubbles as a function of the properties of the fluids used. Laplace's formula

$$\Delta p = \sigma(1/R_1 + 1/R_2)$$

governs the nature of surface separation between any

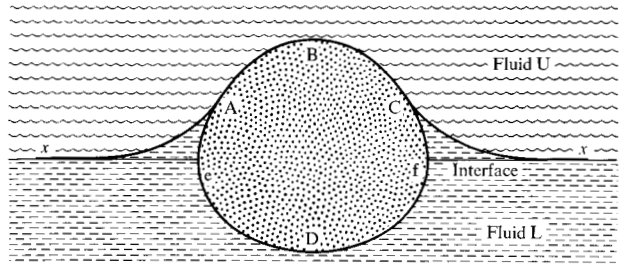

Figure 9 Mathematical model of interface bubble.

Figure 10 Surface of separation and surface tension.

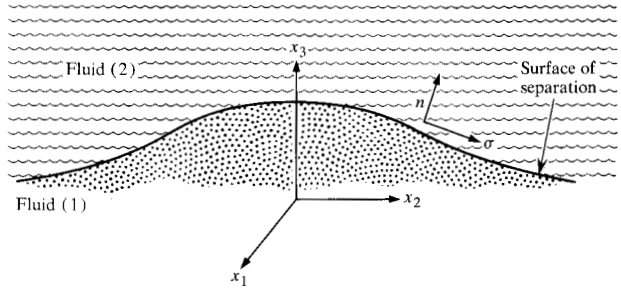

two contiguous media, where Δp is the pressure difference between the two media, R_1 and R_2 the principal radii of curvature at a given point on the surface, and σ the surface tension coefficient between the two media.

In the relation above, the sum of the reciprocals of the radii of curvature can be written in the form of the surface divergence of the unit surface normal, which is equal to the fractional change in surface area per unit distance of normal propagation of the surface. Thus,

$$\Delta p = \sigma\ (\partial n_1/\partial x_1 + \partial n_2/\partial x_2),$$

where the derivatives are to be evaluated on the surface $x_3\,(x_1,x_2) = 0$, and where the unit normal **n** to the surface has the components (see Fig. 10)

$$n_1 = -(1/N)\,(\partial x_3/\partial x_1),$$

$$n_2 = -(1/N)\,(\partial x_3/\partial x_2),$$

$$n_3 = 1/N \text{ and}$$

$$N = [(\partial x_3/\partial x_1)^2 + (\partial x_3/\partial x_2)^2 + 1]^{\frac{1}{2}}.$$

In the case of an axi-symmetric surface for which $x_3 = f(r) = f(x_1^2 + x_2^2)^{1/2}$, it is readily shown that

$$\frac{\partial n_1}{\partial x_1} + \frac{\partial n_2}{\partial x_2} = -\frac{1}{r}\frac{d}{dr}\left[\frac{\mathrm{rf}'}{(1+\mathrm{f}'^2)^{\frac{1}{2}}}\right],$$

so that

$$\Delta p = -\frac{\sigma}{r}\frac{d}{dr}\left[\frac{\mathrm{rf}'}{(1+\mathrm{f}'^2)^{\frac{1}{2}}}\right]. \qquad (1)$$

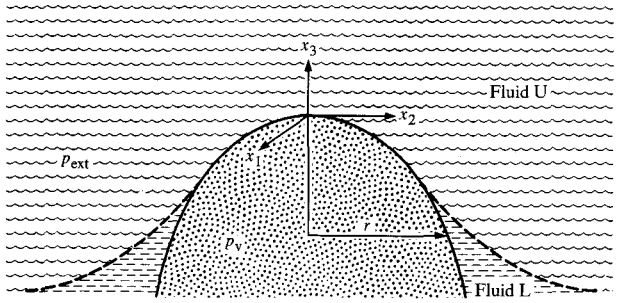

Figure 11 Section of axi-symmetric "dome" surface.

Figure 12 Section of axi-symmetric "cup" surface.

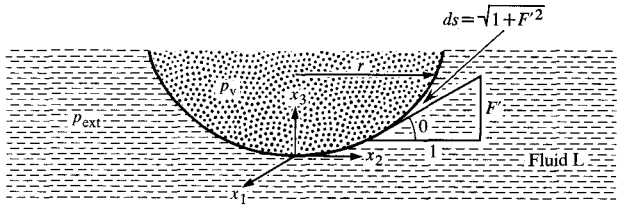

This basic relation is used to find the shapes of the "dome", the "cup", and the "exterior" curves. The curves are then matched subject to the compatibility condition that at the point where the curves join with the same continous slope, the pressure difference Δp must be the same for all surfaces of separation. From the set of possible bubbles, that which has the largest size is found.

We note that the "dome", the "cup" and the "exterior" differ from one another in the way the different surface tensions act on their respective surfaces of separation. For example, in the "exterior" portion in Fig. 9, it is the surface tension between liquids L and U, denoted by σ_{lu}, that acts on the dividing surface. In the "cup" portion, the surface tension of liquid L with respect to its own vapor, σ_l, acts on the dividing surface while in the "dome", the sum of σ_{lu} and σ_l represents the active surface tension.

• *The "dome" solution*

A section of the "dome" surface is shown in Fig. 11. Assume that the pressure distribution exterior to the dome is due to static pressure variation in fluid U alone. Also, assume p_v, the vapor pressure inside the bubble, constant throughout.

Then $\Delta p = (p_v - p_{ext})$.

Now, $p_{ext} = p_{o,d} - \rho_u G x_3$,

where $p_{o,d}$ is the pressure at the origin of the coordinate system chosen in Fig. 7, G is the gravitational constant and ρ_u the density of the upper liquid U. Substituting these relations in Eq. (1), and noting that $x_3 = f(r)$ we obtain

$$p_v - p_{o,d} + \rho_u G f = -\frac{\sigma}{r}\frac{d}{dr}\left[\frac{rf'}{(1+f'^2)^{\frac{1}{2}}}\right],$$

with the boundary condition

$$f(0) = f'(0) = 0$$

where

$$\sigma = \sigma_l + \sigma_{lu}.$$

Now, taking R_d, the radius of curvature at $x_3 = 0$ as the length scale for the dome, and defining

$$F \equiv (f/R_d) \text{ and } R \equiv (r/R_d),$$

the relation above becomes

$$p_v - p_{o,d} + \rho_u G R_d F = -\frac{\sigma}{R_d R}\frac{d}{dR}\left[\frac{RF'}{(1+F'^2)^{\frac{1}{2}}}\right].$$

But

$$p_v - p_{o,d} \approx \frac{2\sigma}{R_d} \quad \text{at } x_3 = 0;$$

$$\therefore \frac{2\sigma}{R_d} + \rho_u G R_d F = -\frac{\sigma}{R_d R}\frac{d}{dR}\left[\frac{RF'}{(1+F'^2)^{\frac{1}{2}}}\right],$$

or

$$2 + \beta_d F = -\frac{1}{R}\frac{d}{dR}\left[\frac{RF'}{(1+F'^2)^{\frac{1}{2}}}\right] \tag{2}$$

with

$$F(0) = F'(0) = 0, \tag{2a}$$

where

$$\beta_d = (\rho_u G R_d^2)/(\sigma_l + \sigma_{lu})$$

is a nondimensional parameter which contains the fluid properties.

The nonlinear second order differential Eq. (2) has been solved on an IBM 7090 computer subject to the boundary conditions given in (2a). The resulting "dome" curves are plotted in Fig. 14 with β_d as the parameter.

• *The "cup" solution*

A section of the "cup" surface is shown in Fig. 12. In this case the normal to the surface is in a direction opposite to x_3. Hence the right hand side of Eq. (2) changes sign. Also, we note that

$$p_{ext} = p_{o,c} - \rho_l G f,$$

where $p_{o,c}$ is the pressure at the origin of the coordinate system shown in Fig. 12. Proceeding as in the subsection on the "dome solution" above, we obtain

$$2 + \beta_c F = \frac{1}{R}\frac{d}{dR}\left[\frac{RF'}{(1+F'^2)^{\frac{1}{2}}}\right]; \tag{3}$$

$$F(0) = F'(0) = 0, \tag{3a}$$

where the new parameter $\beta_c \equiv (\rho_l G R_c^2)/\sigma_l$.

In order to be able to integrate Eq. (3) more readily, it is convenient to put it in the form

$$d\theta/ds = (\beta_c F + 2) - \sin\theta/R. \tag{3b}$$

It has been possible to solve this equation on a computer for values of θ passing through $\pi/2$ by noting that

$$dR = [\cos\theta/(d\theta/ds)]d\theta$$

and $d\theta/ds \approx$ constant $= 1/R_0$ at $\theta = \pi/2$, where $(1/R_0)$ is the curvature.

Thus

$$\int_\theta^{\pi/2} dR = R_0 \int_\theta^{\pi/2} \cos\theta\, d\theta;$$

$$R_{\pi/2} = R_\theta + R_0[1 - \sin\theta].$$

Similarly,

$$dF = [\sin\theta/(d\theta/ds)]\, d\theta$$

so that

$$F_{\pi/2} = F_\theta + R_0\cos\theta.$$

The computer-plotted "cup" curves are given in Fig. 15 with β_c as the parameter.

• *The "exterior" solution*

The pressure difference Δp across the "exterior" surface of separation (Fig. 13) is $\Delta\rho G f$, where $\Delta\rho \equiv (\rho_l - \rho_u)$ so that Eq. (1) becomes:

$$\frac{\Delta\rho G f}{\sigma_{lu}} = \frac{1}{r}\frac{d}{dr}\left[\frac{fr'}{(1+f'^2)^{\frac{1}{2}}}\right].$$

Let

$$\Phi \equiv f(\Delta\rho G/\sigma_{lu})^{\frac{1}{2}}$$

and

$$\zeta \equiv r(\Delta\rho G/\sigma_{lu})^{\frac{1}{2}}$$

With these dimensionless variables, the equation above becomes

$$\Phi = \frac{1}{\zeta}\frac{d}{d\zeta}\left[\frac{\zeta\Phi'}{(1+\Phi'^2)^{\frac{1}{2}}}\right] \tag{4}$$

Equation (4) will assume the form of a modified Bessel's equation when $\Phi' \ll 1$. This is true at large values of ζ since, on physical grounds, the exterior solution curve must extend into the flat interface for $\zeta \to \infty$ (see Fig. 13). Consequently, Eq. (4) has been solved with the boundary conditions

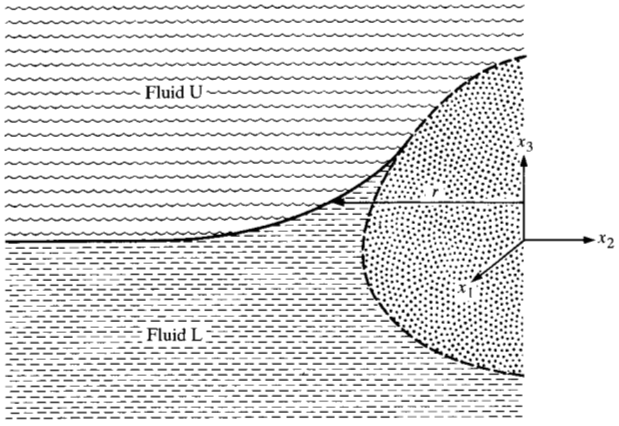

Figure 13 Section of axi-symmetric "exterior" surface.

Figure 14 "Dome" curves.

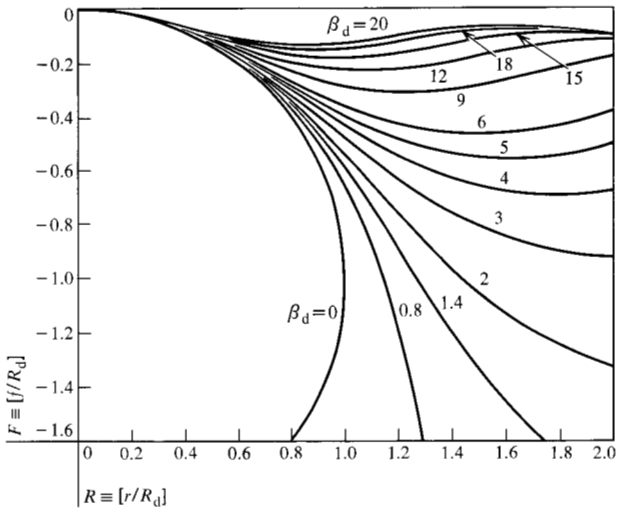

$$\Phi = AK_0(\zeta);$$

$$\Phi' = AK_1(\zeta), \tag{5}$$

where A is a constant and K_0, K_1 are the modified Bessel functions of orders zero and one, respectively.

The computer-plotted exterior curves are shown in Fig. 16 with A as the parameter.

• *Compatibility condition*

The "dome", "cup" and "exterior" curves of Figs. 14, 15 and 16 may now be joined at a match point (Fig. 17) where both the slopes and the abscissa coordinates (r) of all the curves are the same. However, at a match point, the pressure difference Δp across all surfaces of separation must be the same. This "compatibility" condition may be derived by noting that the pressure $p_{o,c}$ at the

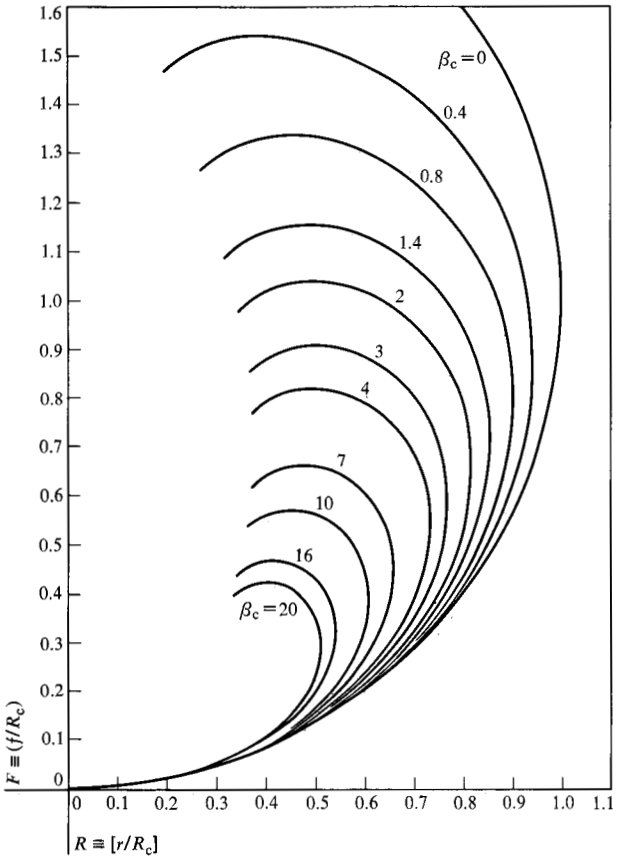

Figure 15 "Cup" curves.

Figure 16 "Exterior" curves.

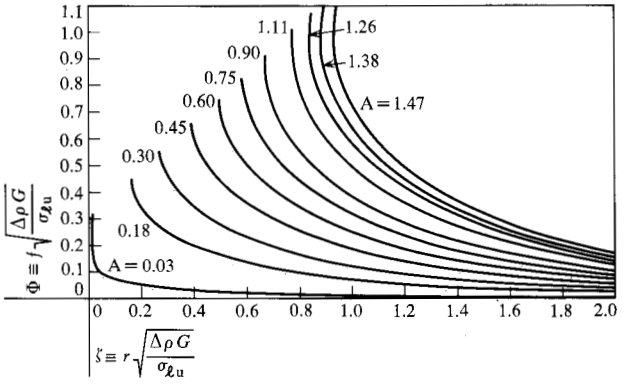

bottom of the "cup" is related to the pressure $p_{o,d}$ at the top of the "dome" by the size of the bubble, which in turn is determined by the surface tensions acting on the surfaces of separation. Assuming that the vapor pressure inside the bubble is constant throughout, we have

$$p_v - p_{o,d} = 2[(\sigma_l + \sigma_{lu})/R_d], \tag{6}$$

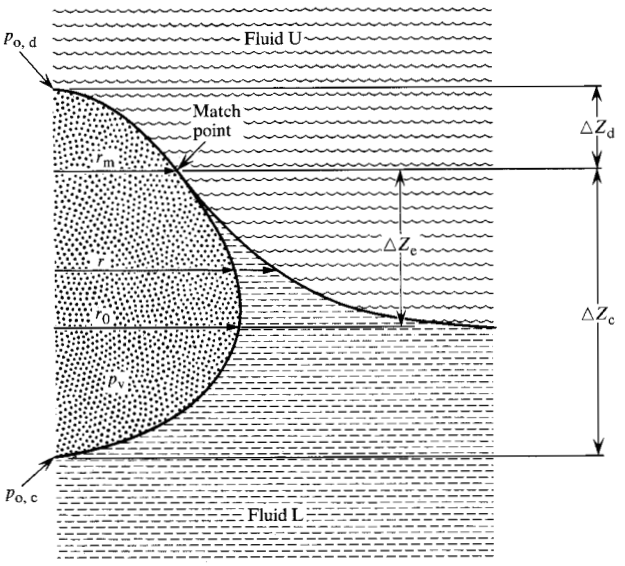

Figure 17 Bubble match.

where R_d is the principal radius of curvature at the top of the "dome." Also,

$$p_v - p_{o,c} = 2\sigma_l/R_c, \tag{7}$$

where R_c is the principal radius of curvature at the bottom of the "cup." Relations (6) and (7) have been stated with the assumption that at the neighborhood of the origin of the cordinate systems in Figs. 11 and 12, the surface is spherical. Subtracting (7) from (6), we obtain

$$p_{o,c} - p_{o,d} = 2\{[(\sigma_l + \sigma_{lu})/R_d] - (\sigma_l/R_c)\}. \tag{8}$$

However, the static pressure $p_{o,c}$ is related to $p_{o,d}$ by

$$p_{o,c} = p_{o,d} + \rho_u G(\Delta Z_d + \Delta Z_e) - \rho_l G \Delta Z_e + \rho_l G \Delta Z_c.$$

Therefore, by Eq. (8), we have the result:

$$2\{[(\sigma + \sigma_{lu})/R_d] - (\sigma_l/R_c)\} = \rho_u G \Delta Z_d + (\rho_u - \rho_l) G \Delta Z_e + \rho_l G \Delta Z_c.$$

With further manipulation of the terms, it can be shown that the above compatibility relationship can be put in the non-dimensional form:

$$\sqrt{\frac{\rho_u}{\rho_l}\left(1 + \frac{\sigma_{lu}}{\sigma_l}\right)}\left[\frac{2}{\sqrt{\beta_d}} - \sqrt{\beta_d}\left(\frac{\Delta Z_d}{R_d}\right) + \sqrt{\frac{\Delta\rho}{\rho_u}\left(\frac{\sigma_{lu}}{\sigma_l + \sigma_{lu}}\right)}\Phi_e\right] = \left[\frac{2}{\sqrt{\beta_c}} + \sqrt{\beta_c}\left(\frac{\Delta Z_c}{R_c}\right)\right] \tag{9}$$

where

$$\Phi_e = \frac{\Delta Z_e}{\sqrt{\frac{\sigma_{lu}}{\Delta\rho G}}}.$$

• *Calculated bubble shapes and sizes*

The nondimensionalized curves of Figs. 14, 15 and 16 can be used to predict the shape and size of interface bubbles in multi-fluid subdued boiling systems using any two liquids. For purposes of illustration, Fig. 18 shows the results obtained for water and FC-78 fluorochemical liquid. The properties of these liquids are given in Table 2.

The procedure for constructing a "compatible" bubble calls for finding those curves from Figs. 14, 15 and 16, with parameters β_d, β_c and A respectively, which satisfy the compatibility equation. For water and FC-78, the equation becomes:

$$1.3113[2/\sqrt{\beta_d} - \sqrt{\beta_d}(\Delta Z_d/R_d) + 0.6786\ \Phi_e] = [2/\sqrt{\beta_c} + \sqrt{\beta_c}(\Delta Z_c/R_c)].$$

Note that the unknowns $(\Delta Z_d/R_d)$, $(\Delta Z_c/R_c)$ and Φ_e in the equation above are the ordinates of the match point for the "dome", "cup" and "exterior" curves respectively. Since the method is simply an iterative one, it will not be given here. The parameters and some of the dimensions for the bubbles shown in Fig. 18 are given in Table 3.

The dashed lines in Fig. 18 depict the growth of a bubble at early stages of development. The solid lines depict the same bubble at a later stage when it is large and raised well above the liquid-liquid interface, just prior to disengagement. Its largest calculated dimension is 0.432 cm. This value agrees well with the bubble diameters measured from high speed motion pictures such as that shown in Fig. 4. Table 4 shows the growth of interface bubble sizes as a function of time.

Conclusions

Multi-fluid subdued boiling offers the advantage of condensing vapor bubbles near their source by a simple superimposition of a second fluid which is immiscible with the boiling liquid. The entrapment of these bubbles between the liquids, their expansion and ascent, their condensation and descent, their contraction and nucleation, and all of these phenomena together, accomplished as they are without appreciable, if any, net vapor generation, suggest interesting cooling concepts and design applications.

The advantages become especially useful where space and geometrical constraints prohibit the installation of a conventional condenser or a compressor in the immediate vicinity of, say, a system requiring vaporization cooling. However, these advantages must be weighed against the requirement of having more than one liquid compatible with the packaging materials.

Not all the mechanisms governing the behavior of multi-fluid subdued boiling phenomena are well understood. Present analysis and experiments suggest that in addition to the individual properties of the fluids, their interfacial properties also determine the overall characteristics of the system. In particular, these properties enter into nondimensional parametric forms by means of which the shapes and sizes of the interface bubbles may be predicted.

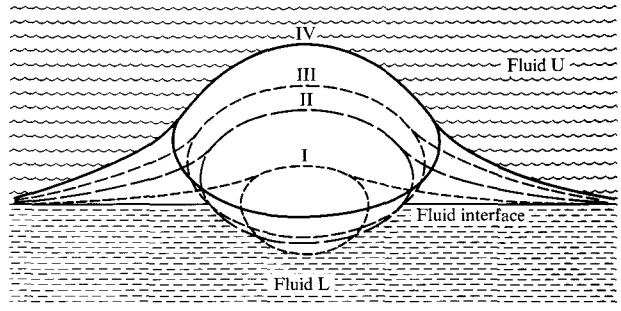

Figure 18 Computer-plotted growth of an interface bubble.

Table 2 Properties of H_2O and FC-78.

Fluids	ρ ($g\text{-}cm^{-3}$)	σ ($dyne\text{-}cm^{-1}$)	$\sigma_{l/u}$ ($dyne\text{-}cm^{-1}$)
Fluid L: (FC-78)	1.7	13	25
Fluid U: (H_2O)	1.0	72	25

Table 3 Parameters of calculated bubbles in Fig. 18.

Bubbles (See Fig. 18)	β_d	β_c	r_m	r_0	ΔZ_d	ΔZ_c	ΔZ_e
			(all values in cm)				
I	1.0	2.0	0.0751	0.102	0.0148	0.1271	0.0386
II	1.2	11.0	0.1578	0.174	0.0637	0.1511	0.0910
III	1.4	20.0	0.1870	0.199	0.0841	0.1561	0.1071
IV	1.2	29.0	0.2100	0.216	0.1239	0.1531	0.1277

Table 4 Interface bubble growth in H_2O/FC-78 system, computed from measurements taken from high speed motion pictures

t (*msec*)	*Bubble diameters (mm)*		
	1	*2*	*3*
200	2.5	1.4	1.4
500	2.9	2.2	2.5
700	4.0	2.9	2.9
900	4.3	3.2	3.5
1100	4.3	3.6	3.6
1400	4.3	4.0	4.0
1600	4.3	4.3	4.3
1800	4.3	4.3	4.3

Acknowledgments

The theoretical analysis was done principally by H. G. Elrod of Columbia University, who was a consultant to IBM in 1966–68 and to whom I express my sincere thanks. I also wish to thank K. Wengier and E. Renner for their competent work in matching bubbles to great quantities of computer print-out data and for conducting the experiments.

References

1. W. M. Rohsenow and H. Choi, *Heat Mass and Momentum Transfer*, Prentice Hall, Englewood Cliffs, N.J. 1961.
2. S. Sideman and T. Taital, *Int. J. Heat and Mass Transfer* **7,** 1273 (1964).
3. J. R. Bragg and J. W. Westwater, "Film Boiling of Immiscible Liquid Mixtures on a Horizontal Plate," *Proc. 4th Int. Heat Transfer Conf.*, Versailles, September 1970.
4. R. Vishanta and P. A. Lottes, "Nucleation and Boiling from a Liquid-Liquid Interface," *1962 Heat Transfer and Fluid Mechanics*, Stanford University Press, 1962.
5. G. Fortuna and S. Sideman, "Direct Contact Heat Transfer Between Immiscible Liquid Layers with Simultaneous Boiling and Stirring," *Chemical Engineering Science* **23,** 1105 (1968). (Printed in Great Britain by Pergamon Press.)
6. J. Isenberg and S. Sideman, "Direct Contact Heat Transfer with Change of Phase: Bubble Condensation in Immiscible Liquids," *Int. J. Heat Mass Transfer* **13,** 997 (1970). (Printed in Great Britain by Pergamon Press.)
7. S. Oktay, "Multi-Fluid Subdued Boiling," *Proc. of the Technical Programme*, International Packaging and Production Conference, Brighton, England, October 1969.
8. J. H. Bleker, S. Oktay and A. F. Schmeckenbecher, "Microelectronic Packaging," *IBM Technical Disclosure Bulletin* **12,** No. 5, October 1969.
9. C. Hansom and J. Ingham, "Direct Liquid-Liquid Heat Exchange," *Brit. J. Chem. Engrg.* **10,** No. 6 (1965).

Received December 21, 1970

S. Oktay is located at the IBM Components Division Laboratory, East Fishkill (Hopewell Junction), New York 12533.